BOLD SIGNAL DECONVOLUTION UNDER UNCERTAIN HÆMODYNAMICS: A SEMI-BLIND APPROACH

Younes Farouj[⋆†]*, F. Işık Karahanoğlu*[‡]*, Dimitri Van De Ville*[⋆†]

[⋆] Institute of Bioengineering, École Polytechnique Federale de Lausanne (EPFL), Switzerland
[†] Department of Radiology and Medical Informatics, University of Geneva (UNIGE), Switzerland
[‡] MGH/HST Athinoula A. Center for Biomedical Imaging, Harvard Medical School, Boston, MA, USA

ABSTRACT

The investigation of spontaneous and evoked neuronal activity from functional Magnetic Resonance Imaging (fMRI) data has come to play a significant role in deepening our understanding of brain function. As this research trend continues, activity detection methods that can adapt to different activation scenarios must be developed. The present work describes a new method for temporal semi-blind deconvolution of fMRI data; i.e., undo temporal signals from the effect of the Hæmodynamic Response Function (HRF), in the absence of information about the timing and duration of neuronal events and under uncertain characterization of cerebral hæmodynamics. A sequential minimization of two functionals is deployed: the first functional recovers activity signals with sparse transients while the second exploits the retrieved activity moments to estimate the Taylor expansion coefficients of the HRF. These coefficients are inherently linked to two values of interests that characterize the hæmodynamics: time-to-peak and the width of the response. We evaluate the performances of the method on synthetic signals before demonstrating its potential on experimental measurements from the visual cortex.

***Index Terms*—** Functional MRI, Joint-estimation, Semi-blind deconvolution, Cerebral hæmodynamics

1. INTRODUCTION

A first and crucial step of fMRI analysis is to detect sufficient evidence of the presence of activation in the acquired blood oxygenated level dependent signals (BOLD). This is often carried out in challenging conditions since one has to deal with noisy time courses and possible model mismatch in the *hæmodynamic response function* (HRF). Joint-estimation is an extension of the well-established general linear model (GLM) based regression, that consists in finding simultaneously the HRF profile and the activated regions responding to a certain stimulus. This approach finds its origins in the work of Makni and collaborators [1, 2] and has several extensions [3, 4]. Recently, Pedregosa *et al.* [5] introduced a regularized version with a rank constraint that imposes the same HRF profile in the time domain. Unfortunately, the use of these methods becomes limited when it comes to studying spontaneous activity. In fact, the absence of explicit tasks makes it hard to find meaningful inputs to drive both the regression and HRF fitting. The exploration of resting-state activity [6] triggered few works that investigate the idea of estimating paradigm-independent activity without imposing a predefined HRF. A non-parametric approach using homomorphic filtering was proposed in [7]. Here, the neural response is assumed to be a high-frequency phenomenon compared to the HRF and thus can be retrieved via high pass filtering. Wu *et al.* [8] conceived a blind deconvolution method for resting-state fMRI data where a threshold is applied to detect possible moments of activation and exploit them to fit a canonical HRF to the data. The main drawback with these methods is their restriction on the regularity of the neuronal signal as only spikes are assumed. Moreover, precise priors on the amplitude of the underlying signal are needed for thresholding steps. There is a gap between, on one hand, methodologies that are linked to the GLM and which can be adjusted to deal with the variability of the HRF, but require a stimulus pattern as an input, and on the other hand, methods that are conceived to catch spontaneous and paradigm-independent activity but are not flexible with respect to the hemodynamics or include too simplistic assumptions on the neuronal signal. The aim of this work is to fill this gap by constructing a semi-blind deconvolution. We revisit the concept of Generalized Total Variation (GTV) [9], which was already used for fMRI deconvolution [10], to incorporate a tailored HRF by its Taylor expansion.

2. MODELING

2.1. From BOLD signals to transients

The measured BOLD signal, $\mathbf{y}$ is considered to be a noisy version of the activity-related signal $\mathbf{x}$ at each time point $t > 0$:

$$\mathbf{y}(t) = \mathbf{x}(t) + \boldsymbol{\varepsilon}_t, \tag{1}$$

where $\boldsymbol{\varepsilon}_t$ are random noise and nuisance components. Typically, one considers that $\mathbf{x}$ is the result of the action of a linear system H whose continuous impulse response is the HRF, $\mathbf{h}$,

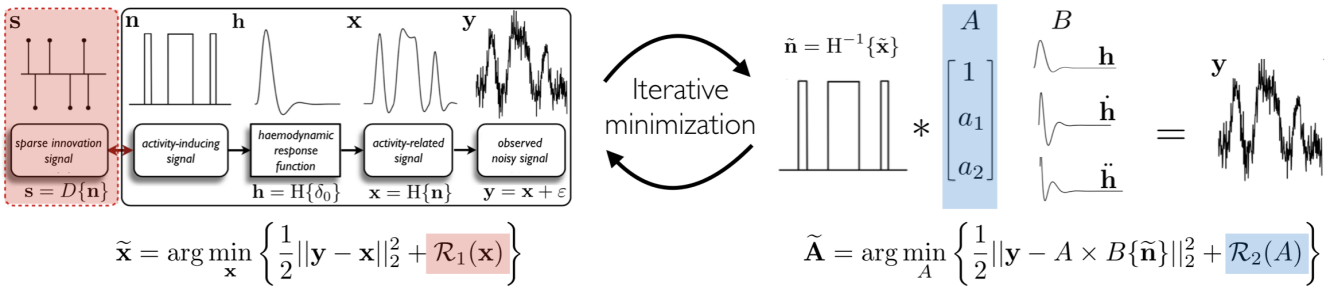

$$\widetilde{\mathbf{x}} = \arg\min_{\mathbf{x}} \left\{ \frac{1}{2}||\mathbf{y} - \mathbf{x}||_2^2 + \mathcal{R}_1(\mathbf{x}) \right\} \qquad \widetilde{\mathbf{A}} = \arg\min_{A} \left\{ \frac{1}{2}||\mathbf{y} - A \times B\{\widetilde{\mathbf{n}}\}||_2^2 + \mathcal{R}_2(A) \right\}$$

Fig. 1: The algorithm alters between activity estimation and HRF correction. The deconvolution step estimates the activity-related signal by imposing a sparsity prior $\mathcal{R}_1$ on the sparse innovation signal. The estimated activity is used to find the Taylor expansion through a regression involving a regularization term $\mathcal{R}_2$ that keeps the corrected HRF close to the initial guess.

on a block-type signal $\mathbf{n}$ showing moments of neural activity. A crucial observation for us is the fact that the derivative of $\mathbf{n}$ is a sparse innovation signal. This sparsity property will be harnessed to recover $\mathbf{x}$ and $\mathbf{n}$ from the knowledge of $\mathbf{y}$.

2.2. HRF characterization

We use the first-order Volterra series approximation of the *Balloon/Windkessel* model [11] to describe the hæmodynamic lag. A distinctive feature of this model is the possibility to define H as the closed form differential operator of the form:

$$\mathrm{H} = \Big(\prod_{i=1}^{N}(D - \beta_i I)\Big)\Big(\prod_{i=1}^{M}(D - \gamma_i I)\Big)^{-1}, \qquad (2)$$

where I is the identity operator, D is the derivative operator and $\boldsymbol{\beta} = (\beta_1, \cdots, \beta_N) \in \mathbb{C}^N$ and $\boldsymbol{\gamma} = (\gamma_1, \cdots, \gamma_M) \in \mathbb{C}^M$ are, respectively, the zeros and poles of H. More precisely, Khalidov *et al.* [12] defined a set of one zero and four poles ($N = 1$ and $M = 4$) such as H mimics the response of the linearized *balloon/windkessel* model. This definition is crucial for us because it allows us to impose a sparsity promoting prior activity transients within the GTV framework. In the sequel, the notations D and H will also refer to discrete counterparts of these operators depending on the context; i.e, when applied to discrete signals. We refer to [9] for discretization details.

3. METHODS

We consider a parametric model in which the empirical HRF is approximated by the Taylor expansion of the *Balloon/Windkessel* model HRF. Here, we chose to use only two degrees of freedom to bring more stability to the overall procedure; we estimate only the coefficients on the first and second derivatives, $\dot{\mathbf{h}}$ and $\ddot{\mathbf{h}}$, while no coefficient is imposed on the first term. This assumption is far from being restrictive. In fact, it is sufficient to consider that the amplitude information is coded in the signal itself and only the time-to-peak and full duration at half maximum (FDHM) are susceptible to vary. In its orthogonalized form, the expansion writes:

$$\widetilde{\mathbf{h}} = \mathbf{h} + a_1\dot{\mathbf{h}}_\perp + a_2\ddot{\mathbf{h}}_\perp, \quad \text{with } (a_1, a_2) \in \mathbb{R} \times \mathbb{R}_+, \qquad (3)$$

where $\dot{\mathbf{h}}_\perp$ and $\ddot{\mathbf{h}}_\perp$ are, respectively, the orthogonalized versions of $\dot{\mathbf{h}}$ and $\ddot{\mathbf{h}}$; i.e, such as the triplet $B = (\mathbf{h}, \dot{\mathbf{h}}_\perp, \ddot{\mathbf{h}}_\perp)$ forms an orthogonal basis. Note that such expansion is similar to the multivariate Taylor expansion: temporal and dispersion derivatives [13], usually used in fMRI studies [8]. Here, we use a classical Taylor expansion (3); i.e, we replace the dispersion derivative by the second-order derivative. This is important for us because it allows to estimate HRFs that can be described by differential operators of the form (2). Note also the estimated HRF have naturally poles and zeros that are different from the original one. We model the semi-blind deconvolution task as a sequential optimization problem (see Fig. 1 for an illustration) in which $\mathbf{x}$ and the vector A of the Taylor expansion coefficients are estimated jointly:

$$\begin{cases} \widetilde{\mathbf{n}} = \widetilde{\mathrm{H}}\{\widetilde{\mathbf{x}}\} \text{ s.t. } \widetilde{\mathbf{x}} = \arg\min_{\mathbf{x}} \left\{ \frac{1}{2}||\mathbf{y} - \mathbf{x}||_2^2 + \mathcal{R}_1(\mathbf{x}) \right\}, & \text{(4a)} \\ \widetilde{A} = \arg\min_{A} \left\{ \frac{1}{2}||\mathbf{y} - A \times B\{\widetilde{\mathbf{n}}\}||_2^2 + \mathcal{R}_2(A) \right\}, & \text{(4b)} \end{cases}$$

where $\widetilde{\mathrm{H}}$ is the linear operator whose impulse response is the corrected HRF, $\widetilde{\mathbf{h}}$. The first term in (4b) aims at learning the operator $\widetilde{\mathrm{H}}$. Because the combination of the two problem (4a) and (4b) is not necessarily convex with respect to both $\mathbf{x}$ and A at the same time, the second term in (4b) is introduced to keep the HRF close from the initial guess. Now, we describe how the regularization terms $\mathcal{R}_1$ and $\mathcal{R}_2$ are constructed before detailing the computation of $\widetilde{\mathrm{H}}$.

3.1. Construction of $\mathcal{R}_1$ and $\mathcal{R}_2$

The regularization term in (4a) aims at controlling the sparsity of the transient moments. Therefore, $\mathcal{R}_1$ is constructed to control the ℓ_1-norm of $\mathbf{s} = \mathrm{D}\{\mathbf{n}\}$. Whenever an estimate of the corrected operator $\widetilde{\mathrm{H}}$ is available, we can use the relationship between $\mathbf{n}$ and $\mathbf{x}$ to construct the GTV regularizer:

$$\mathcal{R}_1(\mathbf{x}) = \mu_1 \, ||D\widetilde{\mathrm{H}}^{-1}\{\mathbf{x}\}||_1, \qquad (5)$$

with $\mu_1 > 0$. Note that such term was already used in the context of fMRI deconvolution [10][14]. On the other hand, $\mathcal{R}_2$ is built to keep the estimated HRF close to the original guess:

$$\mathcal{R}_2(A) = \frac{\mu_2}{2} ||A - A_0||_2^2, \tag{6}$$

with $\mu_2 > 0$ and $A_0 = (1, 0, 0)^T$.

3.2. Updating the HRF operator

The computation of the corrected operator $\widetilde{\mathrm{H}}$ requires using a linear combination of the basis induced by $\mathbf{h}$ and its derivatives. We denote by $\dot{\mathrm{H}}$ and $\ddot{\mathrm{H}}$ the linear operators whose impulse responses are, respectively, $\dot{\mathbf{h}}$ and $\ddot{\mathbf{h}}$. Remember that H is of the form (2), hence $\dot{\mathrm{H}}$ and $\ddot{\mathrm{H}}$ can be constructed by applying first and second order derivatives to H:

$$\dot{\mathrm{H}} = D\,\mathrm{H} = D\Big(\prod_{i=1}^{N}(D - \beta_i I)\Big)\Big(\prod_{i=1}^{M}(D - \gamma_i I)\Big)^{-1}, \tag{7}$$

and

$$\ddot{\mathrm{H}} = D^2\,\mathrm{H} = D^2\Big(\prod_{i=1}^{N}(D - \beta_i I)\Big)\Big(\prod_{i=1}^{M}(D - \gamma_i I)\Big)^{-1}. \tag{8}$$

Their orthogonalized versions will be referred to as $\dot{\mathrm{H}}_\perp$ and $\ddot{\mathrm{H}}_\perp$. We start by noting that $\dot{\mathbf{h}}_\perp$ and $\ddot{\mathbf{h}}_\perp$ can be obtained from $\dot{\mathbf{h}}$ and $\ddot{\mathbf{h}}$ via a Gram-Schmidt process:

$$\begin{cases} \dot{\mathbf{h}}_\perp = \dot{\mathbf{h}} - \frac{\langle \dot{\mathbf{h}}, \mathbf{h}\rangle}{\langle \mathbf{h}, \mathbf{h}\rangle}\mathbf{h} \\ \ddot{\mathbf{h}}_\perp = \ddot{\mathbf{h}} - \frac{\langle \ddot{\mathbf{h}}, \mathbf{h}\rangle}{\langle \mathbf{h}, \mathbf{h}\rangle}\mathbf{h} - \frac{\langle \ddot{\mathbf{h}}, \dot{\mathbf{h}}_\perp\rangle}{\langle \dot{\mathbf{h}}_\perp, \dot{\mathbf{h}}_\perp\rangle}\dot{\mathbf{h}}_\perp. \end{cases} \tag{9}$$

Consequently, the corresponding differential operators are obtained by:

$$\begin{cases} \dot{\mathrm{H}}_\perp = \dot{\mathrm{H}} - \dfrac{\langle \dot{\mathbf{h}}, \mathbf{h}\rangle}{\langle \mathbf{h}, \mathbf{h}\rangle}\mathrm{H} & \text{(10a)} \\ \ddot{\mathrm{H}}_\perp = \ddot{\mathrm{H}} - \dfrac{\langle \ddot{\mathbf{h}}, \mathbf{h}\rangle}{\langle \mathbf{h}, \mathbf{h}\rangle}\mathrm{H} - \dfrac{\langle \ddot{\mathbf{h}}, \dot{\mathbf{h}}_\perp\rangle}{\langle \dot{\mathbf{h}}_\perp, \dot{\mathbf{h}}_\perp\rangle}\dot{\mathrm{H}}_\perp. & \text{(10b)} \end{cases}$$

Finally, we can construct the operator that corresponds to the Taylor approximation $\widetilde{\mathbf{h}}$:

$$\widetilde{\mathrm{H}} = \mathrm{H} + a_1\dot{\mathrm{H}}_\perp + a_2\ddot{\mathrm{H}}_\perp. \tag{11}$$

In order to use this operator in the context of GTV, it has to be of the form (2). This can be done by solving a second order equation to find the new set of zeros of (11).

3.3. Algorithm

The two minimization problems (4a) and (4b) are solved in an iterative manner. At each iteration k, when the current Taylor coefficients are known, a new HRF operator is computed.

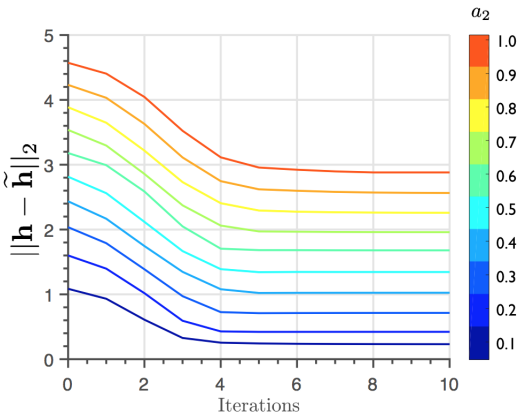

Fig. 2: The evolution of the HRF estimation.

An estimation $\mathbf{x}_k$ of the activity-related signal is then found by solving (4a). The functional therein is not differentiable because of the ℓ_1-term. Finding a solution passes through splitting techniques that separate the non-differentiable term from the quadratic term. Here, we use the fast iterative soft thresholding algorithm (FISTA) [15]. It necessitates to set the regularization parameter μ_1. Here, we opted for a data-driven procedure that consists in defining μ_1 as an estimation of the noise level via the standard deviation of wavelet decomposition coefficients at the finest scale [10]. Once the estimation $\mathbf{x}_k$ is computed, we can solve (4b) to find a new set of Taylor coefficients A by plugging in a new signal $\mathbf{n}_k$. The functional therein, is quadratic and differentiable. The vector A of Taylor expansion coefficients at iteration k is simply given by the zero of the gradient:

$$A = (B\{\mathbf{n}_k\}^T B\{\mathbf{n}_k\} + \mu_2 I)^{-1}(B\{\mathbf{n}_k\}^T\mathbf{y} + \mu_2 A_0). \tag{12}$$

The operator $\widetilde{\mathrm{H}}$ is then updated using the new set of Taylor expansion coefficients and used for the new iteration $k+1$.

4. NUMERICAL EXPERIMENTS

4.1. Synthetic data

A synthetic signal of $600\,s$ long was generated at a realistic sampling rate of 0.5 Hz similar to the one that will be used for experimental tests. It is composed of 10 rectangular pulses with the same amplitude but different durations. The block-signal was convolved with a Taylor expansion (3) of the *HRF*. Here, we varied a_2 in the interval $[0.1, 1]$, while[1] $a_1 = \sqrt{a_2 \times 2} \in [\sqrt{0.2}, \sqrt{2}]$. The output was then corrupted with an additional Gaussian noise such that the final signal-to-noise ratio (SNR) is $10\,dB$. The only parameter that needs user's tuning is the regression regularizer $\mu_2 = 5$. We performed an Oracle search to end up with a value of $\mu = 5$. In

[1] Accordingly to the expected values in a continuous approximation: $h(t - t_0) \approx h(t) - (t - t_0)\dot{h}(t) + \frac{(t-t_0)^2}{2!}\ddot{h}(t)$.

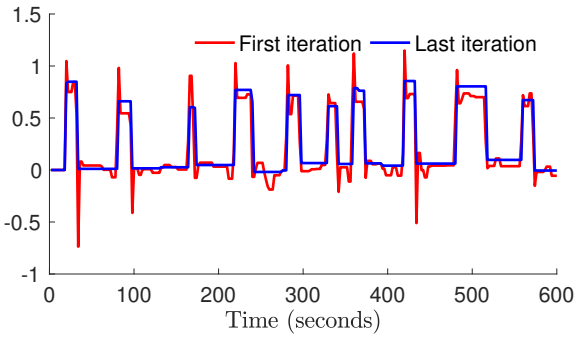

Fig. 3: Deconvolution results in the case $a_2 = 0.2$.

Fig. 2, we display the evolution of the ℓ_2-error measuring the difference between the estimated HRF and the targeted one at each iteration. These curves show the behavior of the algorithm. In fact, from a theoretical point of view, the overall convergence is not guaranteed [16, 17]. Still, it can be observed that the iterative procedure reaches a stationary point after few iterations. In order to appreciate the improvement brought by the iterative process we show the estimated signal and response for the case $a_2 = 0.2$. Fig. 3 provides a visual evaluation of the technique in this configuration. Therein, the driving activity-inducing signals at the first and last iterations are displayed. Note that the activity-inducing signal that was recovered with the corrected HRF is less noisy and more parsimonious.

4.2. Experimental data

To evaluate the method in real case scenarios, we used experimental data acquired on three subjects [10] performing a task involving 9 visual stimuli (8 Hz flickering checkerboard). Each stimulus lasted 1 s and its onset was randomly chosen following a uniform distribution. The fMRI data contains 160 volumes recorded at a TR of $2.04\,s$ with a spatial resolution of $3.25 \times 3.25 \times 3.5$ mm^3. The time courses were realigned to correct for head motion, high-pass filtered and smoothed in the spatial domain via a 3D Gaussian filter (FWHM = 5 mm). For each of the three subject, a single voxel from the visual cortex - without averaging - was used for the experiment. Fig. 4 shows the deconvolution results at the first and last iterations for one of the subjects. The plot shows how the recovered activity-inducing signal capture events with respect to the experimental paradigm. We can also notice the benefit of the HRF correction as the final estimated signals are sparser; closer to the baseline outside activity moments. Another striking observation is the shift that is introduced to the first estimation. This shift makes the onset of activity moments closer to the actual onset of the paradigm in the last estimation. The reason for this is the slow time-to-peak in the original *balloon model* that is compensated by a drift in the estimated signal. Fig. 5 displays the shape of these HRFs

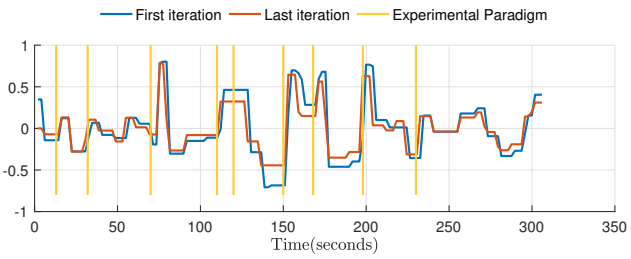

Fig. 4: Estimated activity-inducing signals from subject 2.

in the three subjects. Compared to the original response, we note the presence of an initial dip of about half a second and a stronger undershoot after the peak. In our case this is due to the Taylor approximation. Still, it is worth mentioning that such initial decrease of oxygenation was already observed in fMRI studies[18] and the visual cortex shows particular evidence of its presence [13].

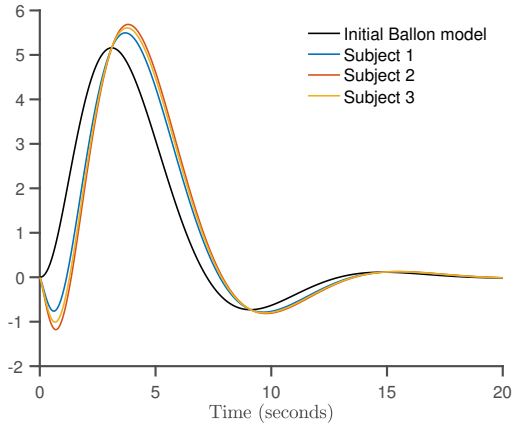

Fig. 5: Estimated HRFs from the three subjects.

5. DISCUSSION & PERSPECTIVES

We exploited the variations in the Taylor approximation of the HRF to construct a semi-blind deconvolution program for fMRI data. The results show how the estimated activity can be enhanced if the initial HRF guess is not optimal. Our model comes with a cost; the space of possible solutions is restricted to linear combinations of first and second derivatives, thus it depends essentially on the initial response. As a consequence some solutions are out of reach, while we hope to estimate responses that are close enough to improve the retrieved signal and observe potential variations between brain regions. The Gaussianity of the noise component is a simplistic assumption. One could consider autoregressive noise models and write the deconvolution problem accordingly [19]. Finally, the algorithm can be used on large datasets to retrieve both stable maps of HRF characteristics and reproducible co-activation patterns.

6. REFERENCES

[1] S. Makni, P. Ciuciu, J. Idier, and J.-B. Poline, "Joint detection-estimation of brain activity in functional mri: a multichannel deconvolution solution," *IEEE Transactions on Signal Processing*, vol. 53, no. 9, pp. 3488–3502, 2005.

[2] S. Makni, J. Idier, T. Vincent, B. Thirion, G. Dehaene-Lambertz, and P. Ciuciu, "A fully bayesian approach to the parcel-based detection-estimation of brain activity in fMRI," *Neuroimage*, vol. 41, no. 3, pp. 941–969, 2008.

[3] T. Vincent, L. Risser, and P. Ciuciu, "Spatially adaptive mixture modeling for analysis of fMRI time series," *IEEE transactions on medical imaging*, vol. 29, no. 4, pp. 1059–1074, 2010.

[4] L. Chaari, T. Vincent, F. Forbes, M. Dojat, and P. Ciuciu, "Fast joint detection-estimation of evoked brain activity in event-related fMRI using a variational approach," *IEEE transactions on Medical Imaging*, vol. 32, no. 5, pp. 821–837, 2013.

[5] F. Pedregosa, M. Eickenberg, P. Ciuciu, B. Thirion, and A. Gramfort, "Data-driven hrf estimation for encoding and decoding models," *NeuroImage*, vol. 104, pp. 209–220, 2015.

[6] B. Biswal, F. Zerrin Yetkin, V. M. Haughton, and J. S. Hyde, "Functional connectivity in the motor cortex of resting human brain using echo-planar mri," *Magnetic resonance in medicine*, vol. 34, no. 4, pp. 537–541, 1995.

[7] K. R. Sreenivasan, M. Havlicek, and G. Deshpande, "Nonparametric hemodynamic deconvolution of fMRI using homomorphic filtering," *IEEE transactions on medical imaging*, vol. 34, no. 5, pp. 1155–1163, 2015.

[8] G.-R. Wu, W. Liao, S. Stramaglia, J.-R. Ding, H. Chen, and D. Marinazzo, "A blind deconvolution approach to recover effective connectivity brain networks from resting state fMRI data," *Medical image analysis*, vol. 17, no. 3, pp. 365–374, 2013.

[9] F. I. Karahanoğlu, İ. Bayram, and D. Van De Ville, "A signal processing approach to generalized 1-d total variation," *IEEE Trans. on Signal Process.*, vol. 59, no. 11, pp. 5265–5274, 2011.

[10] F. I. Karahanoğlu, C.-. Gaudes, F. Lazeyras, and D. Van De Ville, "Total activation: fMRI deconvolution through spatio-temporal regularization," *Neuroimage*, vol. 73, pp. 121–134, 2013.

[11] R. B. Buxton, K. Uludağ, D. J. Dubowitz, and T. T. Liu, "Modeling the hemodynamic response to brain activation," *Neuroimage*, vol. 23, pp. S220–S233, 2004.

[12] I. Khalidov, J. Fadili, F. Lazeyras, D. Van De Ville, and M. Unser, "Activelets: Wavelets for sparse representation of hemodynamic responses," *Signal Processing*, vol. 91, no. 12, pp. 2810–2821, 2011.

[13] K. J. Friston, A. Mechelli, R. Turner, and C. J. Price, "Nonlinear responses in fMRI: the balloon model, volterra kernels, and other hemodynamics," *NeuroImage*, vol. 12, no. 4, pp. 466–477, 2000.

[14] Y. Farouj, F. I. Karahanoğlu, and D. Van De Ville, "Regularized spatiotemporal deconvolution of fMRI data using gray-matter constrained total variation," in *Biomedical Imaging (ISBI 2017), 2017 IEEE 14th International Symposium on*. Ieee, 2017, pp. 472–475.

[15] A. Beck and M. Teboulle, "A fast iterative shrinkage-thresholding algorithm for linear inverse problems," *SIAM journal on imaging sciences*, vol. 2, no. 1, pp. 183–202, 2009.

[16] T. F. Chan and C.-K. Wong, "Total variation blind deconvolution," *IEEE transactions on Image Processing*, vol. 7, no. 3, pp. 370–375, 1998.

[17] ——, "Convergence of the alternating minimization algorithm for blind deconvolution," *Linear Algebra and its Applications*, vol. 316, no. 1-3, pp. 259–285, 2000.

[18] R. S. Menon, S. Ogawa, X. Hu, J. P. Strupp, P. Anderson, and K. Uğurbil, "Bold based functional mri at 4 tesla includes a capillary bed contribution: Echo-planar imaging correlates with previous optical imaging using intrinsic signals," *Magnetic resonance in medicine*, vol. 33, no. 3, pp. 453–459, 1995.

[19] S. Makni, P. Ciuciu, J. Idier, and J.-B. Poline, "Joint detection-estimation of brain activity in fmri using an autoregressive noise model," in *Biomedical Imaging: Nano to Macro, 2006. 3rd IEEE International Symposium on*. IEEE, 2006, pp. 1048–1051.